SCIENCE CHINA
Chemistry

•ARTICLES•

https://doi.org/10.1007/s11426-021-1168-4

Albumin-binding lipid-aptamer conjugates for cancer immunoimaging and immunotherapy

Longlong Tian[1,3], Ming Shao[2], Yimou Gong[2], Yu Chao[2], Ting Wei[2], Kai Yang[4], Qian Chen[2*] & Zhuang Liu[2*]

[1]*Institute of Molecular Medicine, Renji Hospital, School of Medicine, Shanghai Jiao Tong University, Shanghai 200127, China;*
[2]*Institute of Functional Nano and Soft Materials (FUNSOM), Jiangsu Key Laboratory for Carbon-Based Functional Materials and Devices, Soochow University, Suzhou 215123, China;*
[3]*Frontiers Science Center for Rare Isotopes, Lanzhou University, Lanzhou 730000, China;*
[4]*State Key Laboratory of Radiation Medicine and Protection, School of Radiation Medicine and Protection & School for Radiological and Interdisciplinary Sciences (RAD-X), Collaborative Innovation Center of Radiation Medicine of Jiangsu Higher Education Institutions, Soochow University, Suzhou 215123, China*

Received October 3, 2021; accepted November 25, 2021; published online December 21, 2021

Monitoring dynamic changes in tumor immune markers are essential for predicting the therapeutic responses of tumors to immunotherapy, as well as other traditional therapies, such as chemotherapy and radiotherapy. Here, we designed a lipid-aptamer conjugate by employing a C18 chain to modify an aptamer targeting programmed cell death-ligand 1 (C18-apPDL1). The obtained C18-apPDL1 could bind with serum albumin postintravenous injection to achieve prolonged blood circulation and enhanced *in vivo* stability without weakening its binding affinity toward PDL1. C18-apPDL1 labeling with radionuclides, such as ^{99m}Tc, could yield a nuclear imaging agent exhibiting much higher tumor-homing ability than bare aptamer. Notably, such radiolabeled C18-apPDL1 could be utilized to visually monitor the dynamic changes in PDL1 expression postchemotherapy or radiotherapy within a few hours. Additionally, this C18-apPDL1 could offer improved antitumor immune therapeutic responses, which are comparable with those of commercial anti-PDL1 antibodies at the same weight dosage. Thus, this article presented promising lipid-modified aptamers for cancer immunoimaging and immunotherapy.

aptamer, immunoimaging, immunotherapy

Citation: Tian L, Shao M, Gong Y, Chao Y, Wei T, Yang K, Chen Q, Liu Z. Albumin-binding lipid-aptamer conjugates for cancer immunoimaging and immunotherapy. *Sci China Chem*, https://doi.org/10.1007/s11426-021-1168-4

1 Introduction

Immunotherapy, which activates the immune system of a host toward destroying cancer cells, is a promising strategy for treating cancers [1,2]. Although various immunotherapies have achieved great success in the last decades, their therapeutic response rates against solid tumors are yet to be improved [3–5]. As demonstrated, immunotherapy based on the immune checkpoint blockade (ICB) of programmed cell death-1 (PD1) and programmed cell death-ligand 1 (PDL1) depends on the expressions of immune markers, such as PDL1 and $CD8^+$ lymphocyte, in tumors [6,7]. Presently, ICB immunotherapy is generally combined with chemotherapy or radiotherapy in the clinic to achieve optimum responses [8–13]. Histological examinations of different immune markers (PDL1 expressions in the tumor) have become a routine clinical procedure for predicting the therapeutic responses of immunotherapy or its combination therapy [14–17]. However, monitoring of dynamic changes in immune markers *via* noninvasive *in vivo* imaging methods

*Corresponding authors (email: zliu@suda.edu.cn; chenqian@suda.edu.cn)

is necessary because the immune markers in the tumor might change during the therapeutic process [18–21]. Nuclear imaging, a noninvasive imaging method, has been studied as a potential substitute for traditional immunohistochemistry in cancer immunoimaging in clinical and preclinical reports [22–24]. However, radiolabeled ICB antibodies with long blood half-lives generally require several days to achieve the highest tumor imaging contrast, and such time scales do not favor fast diagnosis and prognosis. Moreover, they are incompatible with the short half-lives of most imaging radionuclides [25–28].

Aptamers are single-stranded deoxyribonucleic acid (DNA)/ribonucleic acid (RNA) oligonucleotides that are selected *via* the systematic evolution of ligands by exponential enrichment (SELEX) technology [29–32]. Aptamers, as "chemical antibodies", have exhibited strong affinities for target molecules, demonstrating great potential as substitutes for antibodies [33–36]. However, bare aptamers generally exhibit rather short blood circulation half-lives and low *in vivo* stabilities, which significantly limit their *in vivo* applications [37]. Hence, chemical modifications employing hydrophobic lipid groups have been demonstrated as a valuable approach for significantly improving the pharmacokinetics of therapeutics [38,39]. The hydrophobic lipid tails on such molecules can bind with serum albumin, which is the most abundant serum protein, to achieve prolonged circulation half-lives [40–42]. Furthermore, it has been reported that lipid-oligonucleotide conjugates exhibit high-affinity binding with albumin [43–47].

In this article, a PDL1 aptamer (apPDL1), which was selected as a model molecule [48–50], was further modified with a C18 hydrophobic lipid tail for cancer immunoimaging and immunotherapy. The result indicated that apPDL1 could rapidly bind with albumin after lipid modification without weakening its binding affinity for the PDL1 protein. The C18 lipid-modified apPDL1 (C1-8apPDL1) exhibited a prolonged blood circulation time, as well as enhanced *in vivo* stability, postintravenous (IV) injection owing to its binding with blood albumin. Following the radiolabeling of C18-apPDL1 with ^{99m}Tc (^{99m}Tc-C18-apPDL1), it functioned as a nuclear imaging agent that exhibited greatly enhanced tumor-homing ability, as well as a synchronous increase in the accumulation, in mice that were pretreated with oxaliplatin or irradiation to upregulate the tumor expressing PDL1. This ^{99m}Tc-C18-apPDL1 could visually monitor the changes in the tumor PDL1 expression within a few hours, and this was compatible with the half-life of ^{99m}Tc. Additionally, it greatly delayed tumor growth and was comparable with commercial PDL1 antibodies for cancer immunotherapy at the same weight doses. Thus, this article demonstrated that such a lipid-aptamer conjugate could be a promising candidate for cancer immunoimaging and immunotherapy (Scheme 1).

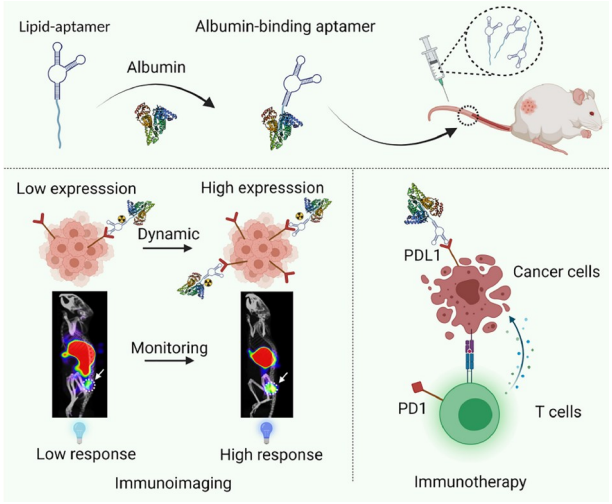

Scheme 1 Schematic of the albumin-binding lipid-oligonucleotides as promising molecules for cancer immunoimaging and immunotherapy. Lipid-aptamer could rapidly bind with blood albumin postintravenous injection to enhance stability and prolong the blood circulation time. The radiolabeled lipid-aptamer could monitor the dynamic changes in the tumor immune markers. Concurrently, lipid-aptamer could block the PD1 and PDL1 interaction for cancer immunotherapy (color online).

2 Experimental

2.1 Materials

2-Cyanoethyl-*N*,*N*-diisopropyloctadecylphosphoramidite was purchased from Beijing HWRK Chem. Co., Ltd. (China). The DNA aptamers were purchased from Sangon Biotech Co., Ltd. (China). Diethylenetriaminepentaacetic acid (*p*-SCN-Bn-DTPA) was purchased from Macrocyclics, Inc. (USA). Human serum albumin (HSA) was purchased from Sigma-Aldrich (USA). Na^{99m}TcO4 was purchased from Shanghai GMS Pharmaceutical Co., Ltd. (China). Oxaliplatin was purchased from Bide Pharmatech Ltd. (China). Enzyme-linked immunosorbent assay (ELISA) was purchased from Invitrogen Corporation (USA). Further, lactose, paraformaldehyde, *N*,*N*-diisopropylethylamine, $NaHCO_3$, $MgSO_4$, triethylamine, octadecanol, and dichloromethane were purchased from Sinopharm Chemical Reagent Co., Ltd. (China).

2.2 Aptamer synthesis

Lipid phosphoramidite was synthesized following a previous report [47]. *N*,*N*-diisopropylethylamine (350 μL, 2 mmol) was added into octadecanol (294 mg, dissolved in dichloromethane), and the mixture was protected in N_2 gas and cooled in an ice bath. Next, 2-cyanoethyl-*N*,*N*-diisopropyloctadecylphosphoramidite (350 μL), which had been dissolved in dichloromethane, was added by employing a syringe. After stirring for 3 h, the mixture was washed with $NaHCO_3$, dried over $MgSO_4$ (solid), and further purified on triethylamine-alkalized silica gel (ethyl acetate/hexanes/1%

triethylamine as the mobile phase). Lipid phosphoramidite (the clear yellow oil) was stored at −20 °C for further solid-phase DNA synthesis of lipid-aptamer (Table S1 presents the DNA sequence, Supporting information online). Next, diethylenetriaminepentaacetic acid (*p*-SCN-Bn-DTPA) was dissolved in a phosphate buffer solution (the pH was adjusted to 8 with a NaOH solution). After adding an amino-group-modified aptamer (NH_2-aptamer) at a mole ratio of 5:1 (*p*-SCN-Bn-DTPA:NH_2), the mixture was stirred overnight at 55 °C. The DTPA-conjugated aptamer (DTPA-aptamer) was purified *via* centrifugal filtration by employing Amicon filters (10 kDa) to remove excess *p*-SCN-Bn-DTPA.

2.3 Albumin binding

Here, 0.5 μL of 100 μM apPDL1 or C18-apPDL1 in a phosphate buffer solution was added in 5 μL of an HSA solution (40 mg/mL in a phosphate buffer). The mixture was immediately loaded and subjected to polyacrylamide gel electrophoresis (PAGE). The electrophoretic parameters were 2 μL of the loading buffer, 8% PAGE, a Tris-acetate-EDTA (TAE) running buffer, and 100 V for 40 min. The gel bands were stained with GelRed and imaged with an Amersham Imager 600.

2.4 *In vitro* cellular binding

A total of 5×10^4 cells (B16, CT26, and C1498 cells) were incubated with 200 nM 5-carboxyfluorescein (FAM) labeled aptamers (apPDL1, C18-apPDL1, and lipid-modified random sequence (C18-apRAN)) in 100 μL of the buffer containing 10% fetal bovine serum (FBS) for 1 h. After two rounds of washing, the cancer cells were resuspended for flow cytometry analysis (BD Accuri C6). For confocal imaging, the CT26 cells were adhered to a cell culture dish and incubated with 200 nM FAM-labeled C18-apPDL1 for 1 h, after which they were imaged *via* confocal microscopy (ZEISS LSM 800 with Airyscan).

2.5 Animal model

Female Balb/c and C57BL/6 mice (Nanjing Peng Sheng Biological Technology Co., Ltd., China) were utilized under standard protocols that were approved by the Laboratory Animal Center at Soochow University (No. SYXK(su)2017-0049). To develop the tumor model, 1×10^6 CT26 or B16 cells in 50 μL of phosphate-buffered saline (PBS) were subcutaneously injected into the back of each mouse.

2.6 Blood circulation

Healthy Balb/c mice were intravenously injected with Cy5-labeled apPDL1 or C18-apPDL1, after which blood (~20 μL) was drawn from the right orbital venous plexus and weighted at different times postinjection. Moreover, the blood was lysed with a red blood cell lysis buffer to quantitatively measure fluorescence intensity and calculate pharmacokinetics.

2.7 *In vivo* and *ex vivo* fluorescence imaging

The Balb/c mice bearing the CT26 tumor (~150 mm^3) were intravenously injected with Cy5-labeled apPDL1, C18-apPDL1, or C18-apRAN (1 nmol per mouse). At different times postinjection, the mice were imaged with small animal imaging systems (IVIS Lumina LT Series III, PerkinElmer). At 6 h postinjection, the mice were sacrificed, and their major organs and tumors were collected for *ex vivo* imaging. Afterward, the tumors were embedded in optimum cutting temperature compound gel at −80 °C for the frozen section technique. Subsequently, the tumor slices were fixed with 4% paraformaldehyde and stained with DAPI for confocal microscopy imaging.

2.8 Radiolabeling

Here, 5 mCi of $Na^{99m}TcO4$ (Shanghai GMS Pharmaceutical Co., Ltd.) and 100 μL of 10 mg/mL $NaBH_4$ (employed as the reductant) were added into DTPA-aptamer. After shaking for 20 min, the free Tc and excess reductant were removed *via* centrifugal filtration until no radioactivity could be detected in the filtration solution, thus yielding the ^{99m}Tc-labeled aptamers.

2.9 Single-photon emission computed tomography (SPECT) imaging

The Balb/c mice bearing the CT26 tumors (~200 mm^3) were intravenously injected with ^{99m}Tc-apPDL1, ^{99m}Tc-C18-apPDL1, or ^{99m}Tc-C18-apRAN (0.3 mCi). At 0.5, 2, 6, and 12 h postinjection, the mice were imaged with a small animal SPECT (MILabs, Utrecht, the Netherlands) imaging system. These mice were treated with blank 10% lactose (intravenous injection), oxaliplatin (3 mg/kg), or X-ray irradiation (8 Gy local treatment). Two days after the treatment, the mice were intravenously injected with ^{99m}Tc-C18-apPDL1 (0.3 mCi) and imaged at 0.5, 2, 4, 6, 8, and 12 h postinjection.

2.10 Biodistribution

The Balb/c mice bearing the CT26 tumors (~150 mm^3) were intravenously injected with ^{99m}Tc-apPDL1, ^{99m}Tc-C18-apPDL1, or ^{99m}Tc-C18-apRAN (0.1 mCi). At 24 h post-injection, the mice were sacrificed, after which all major organs and tumors were collected and weighed. The radioactivities of the samples were measured with a gamma

counter, after which the mice were pretreated with blank 10% lactose, X-ray irradiation (8 Gy), or oxaliplatin (3 mg/kg). Two days after the treatment, the tumors were collected from the mice and fixed with 4% paraformaldehyde for immunohistochemistry assay to evaluate the expression of PDL1. Concurrently, the mice were intravenously injected with ^{99m}Tc-C18-apPDL1 (0.1 mCi) after the treatments and were sacrificed 24 h postinjection. Afterward, all major organs and tumors were collected and weighed. The radioactivities of the samples were measured with a gamma counter (LB211, Berthold Technologies Gmbh & Co. KG)

2.11 *In vivo* cancer therapy

Twenty-four C57BL/6 mice bearing B16 tumors (~30 mm^3) were randomly divided into four groups (n = 6), namely, the PBS, apPDL1, anti-PDL1 (Bioxcell, BE0101), and C18-apPDL1 groups. Treatments were repeated every other day five times at a dosage of 1 nmol aptamer or 15 μg of the antibody. The tumor volumes were measured with a caliper and calculated according to the following standard formula: 0.5 × length × width^2. Three days after the fifth treatment, one mouse from each group was sacrificed, and all of their major organs (hearts, livers, spleens, lungs, and kidneys) and tumors were collected and fixed with 4% paraformaldehyde for hematoxylin and eosin (H&E), as well as terminal deoxynucleotidyl transferase dUTP nick end labeling (TUNEL) staining (Wuhan Servicebio Technology Co., Ltd., China).

2.12 Evaluation of the tumor immune microenvironment

Twenty C57BL/6 mice bearing B16 tumors (~30 mm^3) were randomly divided into four groups (n = 5) as described above. These mice were sacrificed on the third day after the fifth treatment, and their tumors and blood were collected. Next, single-cell suspensions of the tumors were prepared with a homogenizer, and the tumor cells were stained for flow cytometry analysis (CD3-FITC, CD4-APC, and CD8-PE). The tumor necrosis factor alpha (TNF-α) and interferon gamma (IFN-γ) levels in the mice sera and tumor supernatants were measured with the ELISA assays.

3 Results and discussion

To obtain the lipid-modified apPDL1 (C18-apPDL1) *via* the solid-phase DNA synthesis method, intermediate lipid phosphoramidite was synthesized by employing octadecanol and phosphoramidite following previous reports [47] (Figure 1a). The structure of lipid phosphoramidite was confirmed *via* proton and carbon-13 nuclear magnetic resonance spectrometry (^{1}H and ^{13}C NMR, respectively), as well as high-resolution electrospray ionization mass spectrometry (HR-ESI-MS) (Figures S1–S3, Supporting Information online). Thereafter, the interaction between the obtained C18-apPDL1 and albumin was investigated. Further, to simulate the intravenous injection of lipid-oligonucleotides, apPDL1 or C18-apPDL1 was mixed with 40 mg/mL HSA (the approximate concentration in serum), after which the mixture was loaded and subjected to PAGE. The gel bands indicated that albumin did not change the electrophoresis behavior of bare apPDL1, indicating that bare apPDL1 could not bind with albumin (Figure 1b). In marked contrast, the migration of C18-apPDL1 was significantly delayed after the addition

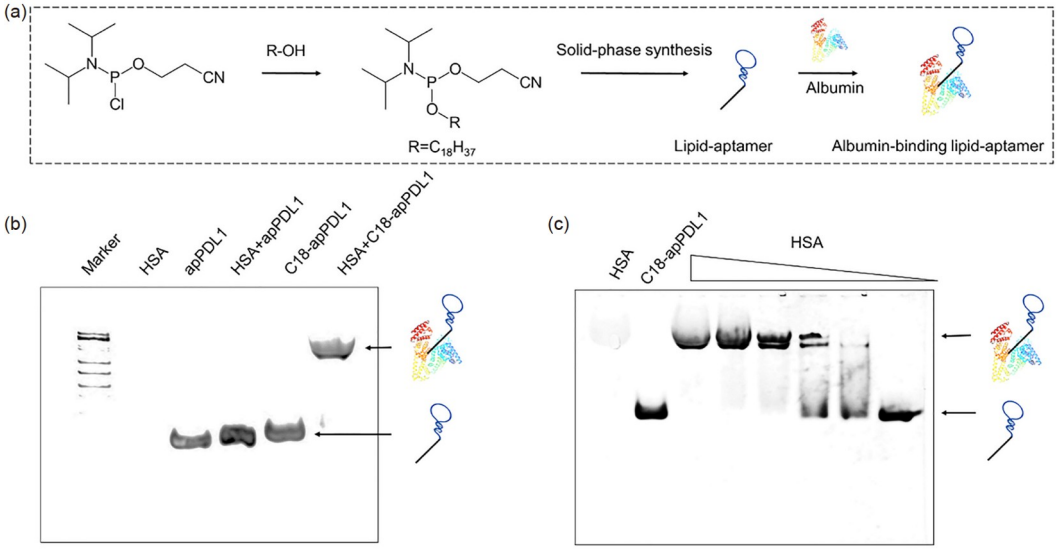

Figure 1 Synthesis of the albumin-binding lipid-aptamer. (a) Schematic of the solid-phase synthesis of the albumin-binding lipid-aptamer. (b) PAGE analyses of apPDL1 and C18-apPDL1 after the incubation with HSA. The delayed gel band of C18-apPDL1 after the addition of HSA indicated the strong interaction between C18-apPDL1 and HSA. (c) PAGE analysis of C18-apPDL1 after the incubation with different concentrations of HSA (color online).

of albumin, thus demonstrating the binding between lipid-oligonucleotides and albumin. The slightly enlarged size of albumin following the addition of lipid-oligonucleotides further proved their binding (Figure S4). Further, it was proven that C18-apPDL1 and albumin exhibited a concentration-dependent interaction (Figure 1c). C18-apPDL1 was incubated with fresh mouse serum and was subsequently loaded for PAGE. Compared with the bare apPDL1, which gradually degraded in 2 h, C18-apPDL1 remained stable 12 h after the incubation (Figure S5). Therefore, C18-apPDL1 exhibited much higher stability than bare apPDL1 probably because it bonded tightly with albumin to prevent the degradation of the oligonucleotides by nuclease.

Next, we wondered whether lipid modification would weaken the cell-binding affinity of the aptamer. To elucidate this, B16 mouse melanoma cells, CT26 murine colon carcinoma cells, and C1498 mouse leukemia cells were incubated with FAM-labeled bare apPDL1, C18-apPDL1, or C18-apRAN in the binding buffer containing 10% FBS. Flow cytometry analysis results (Figure 2a–c) revealed that C18-apRAN exhibited negligible cell binding whereas C18-apPDL1 exhibited strong cell binding that was comparable

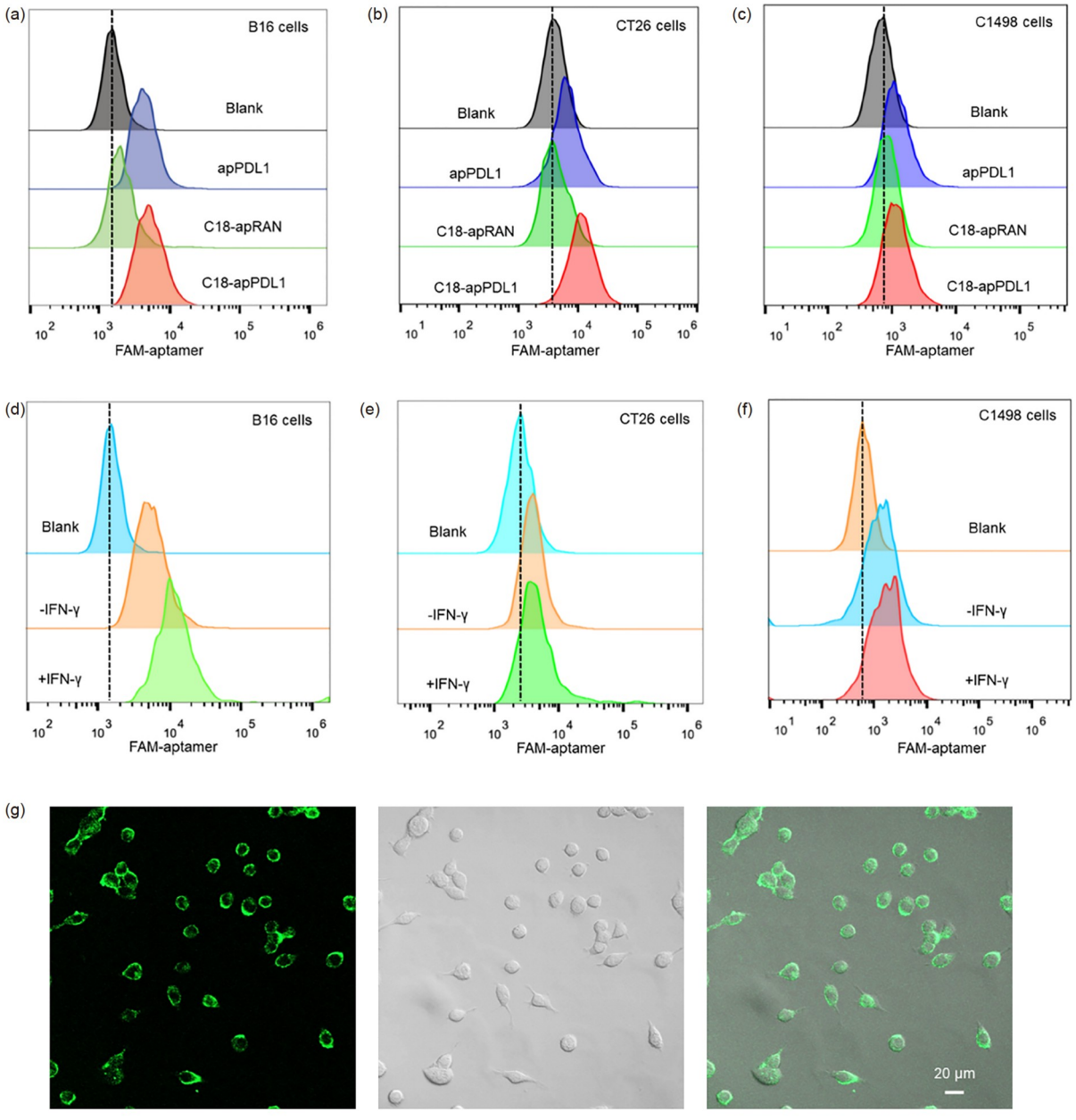

Figure 2 *In vitro* cancer cell binding of the aptamer. Flow cytometry analyses of the B16 (a), CT26 (b), and C1498 (c) cells after the incubation with 200 nM FAM-labeled apPDL1, C18-apPDL1, and C18-apRAN. Flow cytometry analyses of the B16 (d), CT26 (e), and C1498 (f) cells after the incubation with 200 nM FAM-labeled C18-apPDL1. The cancer cells were pretreated with/without IFN-γ. (g) Confocal images of the CT26 cells after the incubation with 200 nM FAM-labeled C18-apPDL1 (color online).

with that of bare apPDL1 for all tested cell lines. To further verify the strong cell-binding affinities of C18-apPDL1 that was attributed to the interaction between the apPDL1 and PDL1 proteins on the surface of the cell membrane, the B16, CT26, and C1498 cells were stimulated by IFN-γ, which could facilitate the upregulation of PDL1 expression (Figure S6). Thereafter, the cancer cells exhibiting low and high PDL1 expressions were incubated with the FAM-labeled C18-apPDL1 and analyzed *via* flow cytometry. The results indicated that the cell binding of C18-apPDL1 correlated positively with the PDL1 expression on those cells (Figure 2d–f and Figure S7), and the confocal images further indicated visually that C18-apPDL1 was not engulfed by the cancer cells; it was mainly bound to the cell surface (Figure 2g).

Next, the *in vivo* behaviors of lipid-oligonucleotides were studied. After the intravenous injection, the calculated half-lives of apPDL1 and C18-apPDL1 were 0.125 and 0.456 h, respectively, demonstrating that C18-apPDL1 exhibited much longer blood circulation time than bare apPDL1 owing to the albumin-binding ability of C18-apPDL1 (Figure 3a). The *in vivo* fluorescence images (Figure 3b) revealed that much stronger fluorescence signals were observed in the mouse tumors after the intravenous injection of Cy5-labeled lipid-aptamer than in the mice injected with Cy5-labeled free aptamer. The *ex vivo* imaging of the major organs of the mice 24 h postinjection revealed the weak and strong signals in the tumors and kidneys of the mice after the injection of bare apPDL1, respectively (Figure 3c). Conversely, strong and weak signals were observed in the tumors and kidneys of the mice after the injection of lipid-aptamer, respectively, indicating that the *in vivo* behavior of the oligonucleotides would be greatly changed after lipid modification. Compared with the bare apPDL1 that could be rapidly eliminated from the kidney owing to its low molecular weight, C18-apRAN, following its binding with blood albumin, could accumulate in the tumor owing to the enhanced permeability and retention effect. Thus, C18-apPDL1 demonstrating molecular targeting and albumin-binding abilities exhibited the highest tumor accumulation, and the notable fluorescence signals observed in the confocal images of the tumor slices further confirmed its superior tumor-targeting ability (Figure 3d).

Motivated by the excellent tumor-targeting ability of C18-apPDL1, we wondered whether the radiolabeled C18-

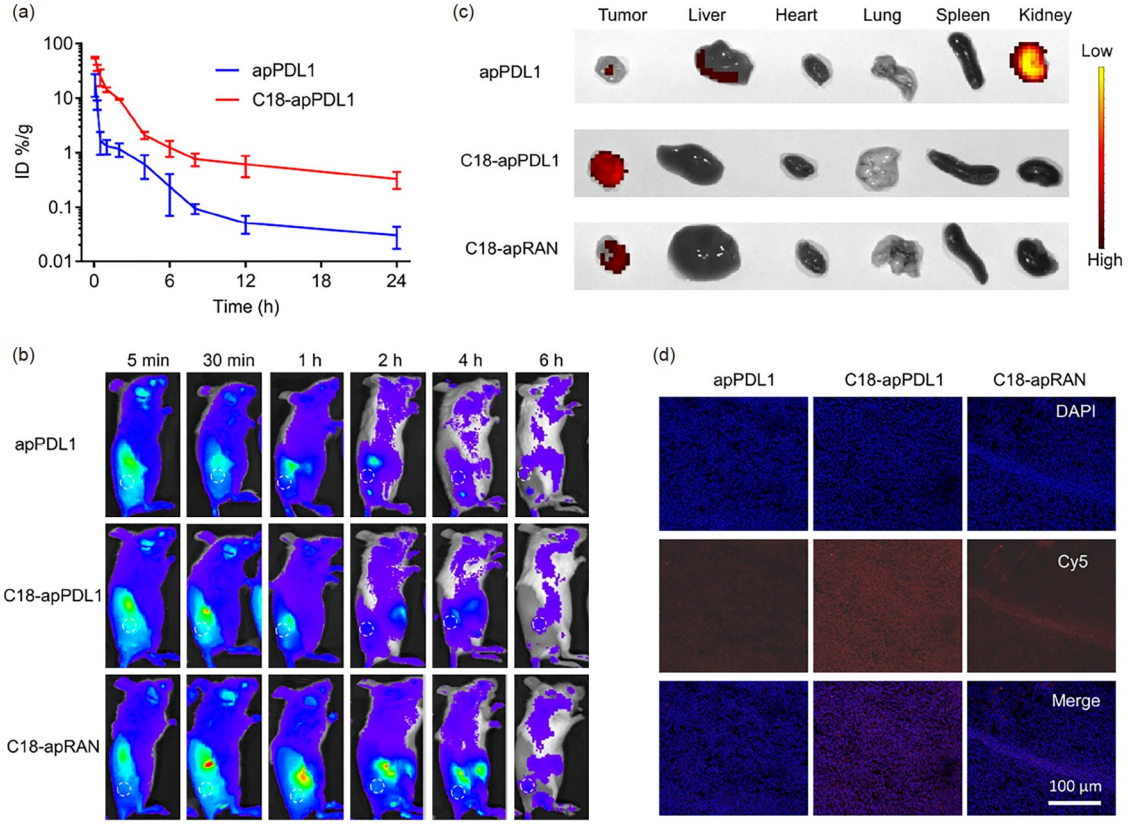

Figure 3 *In vivo* behavior of C18-apPDL1 based on fluorescence imaging in CT26 tumor-bearing Balb/c mice. (a) Blood circulation profiles of Cy5-labeled ap-PDL1 and C18-apPDL1 postintravenous injection. (b) *In vivo* fluorescence images of the mice at different times (5 min, 30 min, 1 h, 2 h, 4 h, and 6 h) postintravenous injection of Cy5-labeled apPDL1, C18-apPDL1, and C18-apRAN (1 nmol). The white-dotted circles represent the tumors. (c) *Ex vivo* fluorescence images of the major organs 24 h postintravenous injec-tions of Cy5-labeled apPDL1, C18-apPDL1, and C18-apRAN (1 nmol). (d) Confocal images of the tumor slices of the mice postintravenous injection of the Cy5-labeled apPDL1, C18-apPDL1, and C18-apRAN (1 nmol). The cell nuclei were stained with DAPI (blue) (color online).

apPDL1 could act as a nuclear imaging agent. Here, DTPA as a chelating radionuclide for ^{99m}Tc labeling was conjugated to the oligonucleotides *via* the chemical reaction between isothiocyanate and the amino group (Figure 4a and Figure S8). The mice bearing the subcutaneous CT26 tumors were intravenously injected with the ^{99m}Tc-labeled oligonucleotides. These mice were imaged with a small animal SPECT imaging system at different times postinjection. Consistent with the above fluorescence imaging results, much higher signals were observed in the tumors of the mice that were treated with C18-apPDL1 than in those of the mice that were treated with apPDL1 and C18-apRAN (Figure 4b). The mice were sacrificed 24 h postinjection. The major organs and tumors were collected and weighed to calculate quantitative biodistribution. The ^{99m}Tc-labeled aptamers mainly accumulated in their livers, spleens, and kidneys, indicating that aptamer could be captured by reticuloendothelial systems and eliminated through the kidney. Notably, the tumor uptakes of apPDL1, C18-apPDL1, and C18-apRAN were 0.45%ID/g, 0.88%ID/g, and 0.41%ID/g, respectively (Figure 4c), demonstrating that the tumor uptake of C18-apPDL1 was almost two times that of free apPDL1.

It is well known that immunotherapy depends on the expression of the immune markers in tumors. Thus, to predict therapeutic responses, radiolabeled C18-apPDL1 instead of histological examination was employed to monitor the changes in the immune markers posttherapy (Figure 4d). The mice bearing the subcutaneous CT26 tumors were subjected to chemotherapy (oxaliplatin) or radiotherapy (X-ray irradiation) treatments. Two days after the treatments, the tumors were collected for immunohistochemical staining of PDL1 expression. The micrograph (Figure 4e) and statistical

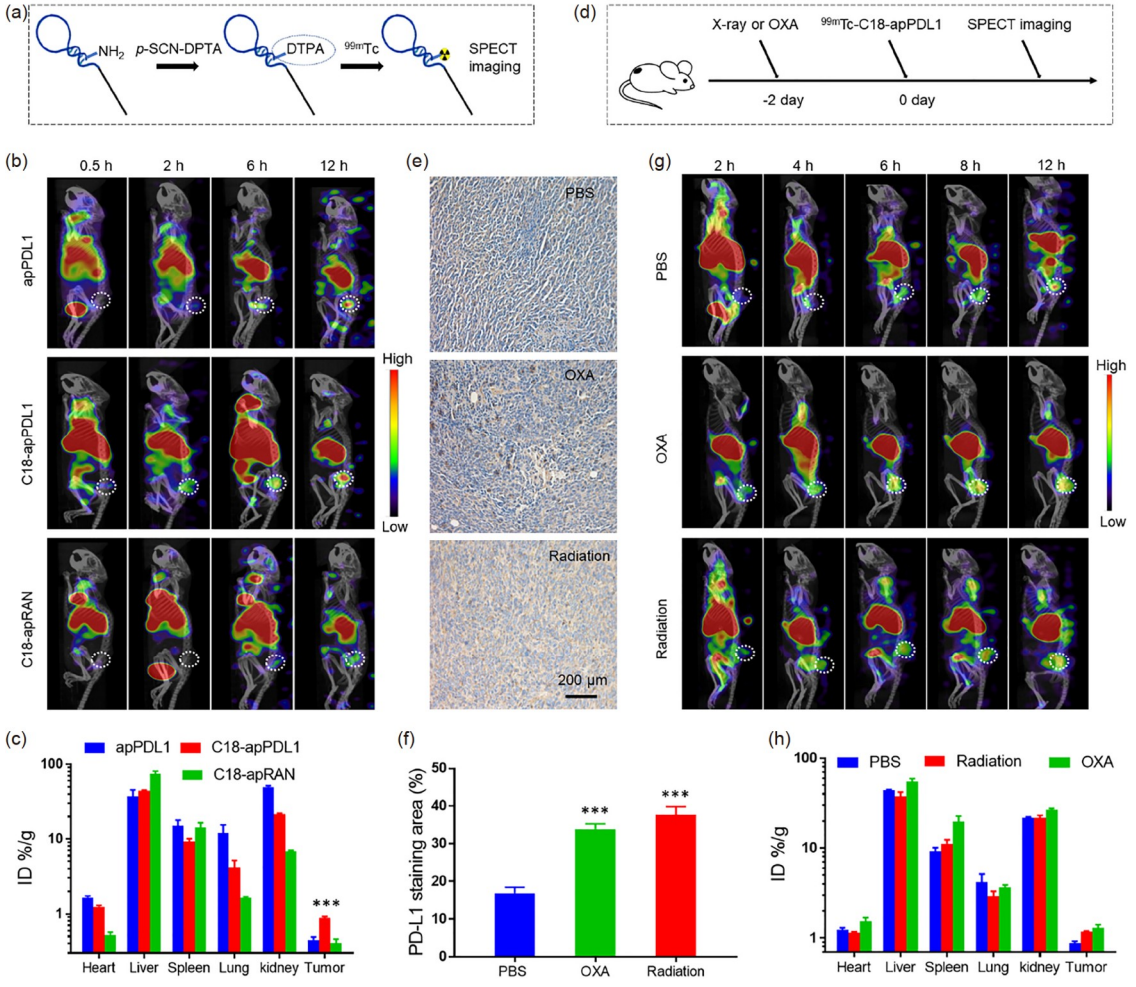

Figure 4 *In vivo* nuclear imaging with C18-apPDL1 in CT26 tumor-bearing Balb/c mice. (a) Schematic of the chelation of the DTPA-conjugated aptamer with ^{99m}Tc for SPECT imaging. (b) SPECT imaging and (c) quantitative biodistributions of ^{99m}Tc-labeled apPDL1, C18-apPDL1, and C18-apRAN. (d) Schematic of ^{99m}Tc-labeled C18-apPDL1 for monitoring PDL1 expression after radiotherapy or chemotherapy. (e) Micrographs and (f) statistics of the immunohistochemical staining of PDL1 expression in the tumor two days after the radiation (X-ray, 8 Gy) or oxaliplatin (OXA, 3 mg/kg) treatment. (g) SPECT imaging of the pretreated mice at different times after the injection of ^{99m}Tc-labeled C18-apPDL1. (h) Biodistribution of ^{99m}Tc-labeled C18-apPDL1 in the tumor of the mice that were pretreated with radiation or OXA. The mice that were pretreated with PBS were employed as the blank control. The white-dotted circles represent the tumors. The error bars denote the standard error of the mean (SEM), and the *P* values were calculated by ANOVA (***$p < 0.001$) (color online).

(Figure 4f) data proved that oxaliplatin (OXA) and irradiation could upregulate PDL1 expression in tumors. Simultaneously, the pretreated mice were intravenously injected with ^{99m}Tc-labeled C18-apPDL1 and subsequently imaged by SPECT (Figure 4g). Compared with the untreated tumors, much stronger SPECT signals were observed in the tumors of the mice that were treated with oxaliplatin or X-ray radiation, indicating that the tumor uptake of ^{99m}Tc-labeled C18-apPDL1 correlated positively with PDL1 expression. After 24 h of injecting ^{99m}Tc-C18-apPDL1, quantitative biodistribution further confirmed that the therapy-induced upregulation of PDL1 expression was reflected by the improved accumulation of C18-apPDL1 (Figure 4h). Overall, these results demonstrated that radiolabeled C18-apPDL1 could monitor the changes in the PDL1 expressions in tumors.

Inspired by the excellent binding between C18-apPDL1 and cancer cell surface PDL1 proteins, we further wondered whether C18-apPDL1 could be an alternative to commercial anti-PDL1 antibodies for ICB therapy. The mice bearing B16 tumors were randomly divided into four groups and were treated with PBS, bare apPDL1, anti-PDL1 antibody, or C18-apPDL1 every other day five times (Figure 5a). The tumor growth curves (Figure 5b and Figure S9) revealed that the bare apPDL1 group exhibited negligible tumor growth inhibition compared with the control group. The commercial anti-PDL1 antibody also exhibited considerable tumor growth inhibition ability. Interestingly, C18-apPDL1 with an equal mass dose with the anti-PDL1 antibody exhibited comparable tumor growth inhibition ability and significantly increased the survival times of the mice (Figure 5c). The H&E- and TUNEL-stained tumor slices from the mice also revealed that the cancer cells were significantly damaged post-C18-apPDL1 treatment (Figure 5d). Additionally, no evident damage was observed in the main organs of the mice posttherapy (Figure 5e), indicating the safety of C18-apPDL1 (Figure S10).

To further clarify its excellent therapeutic efficacy, the tumor immune microenvironment was evaluated post-C18-apPDL1 treatment (Figure 6a). The results of the flow cytometry analysis (Figure S11) indicated that the infiltration of the $CD3^+$ (Figure 6b), $CD4^+$ (Figure 6c), and $CD8^+$ (Figure 6d) T lymphocytes in the tumors increased only slightly post-apPDL1 treatment compared with that in the control group. In marked contrast, the evidently increased tumor infiltration of those T lymphocytes was observed post-C18-apPDL1 and anti-PDL1 antibody treatments. The percentages of the $CD8^+$ lymphocytes among the $CD3^+$ cells were also increased post-C18-apPDL1 and anti-PDL1 antibody treatments (Figures 6e and 6f). IFN-γ and TNF-α, two

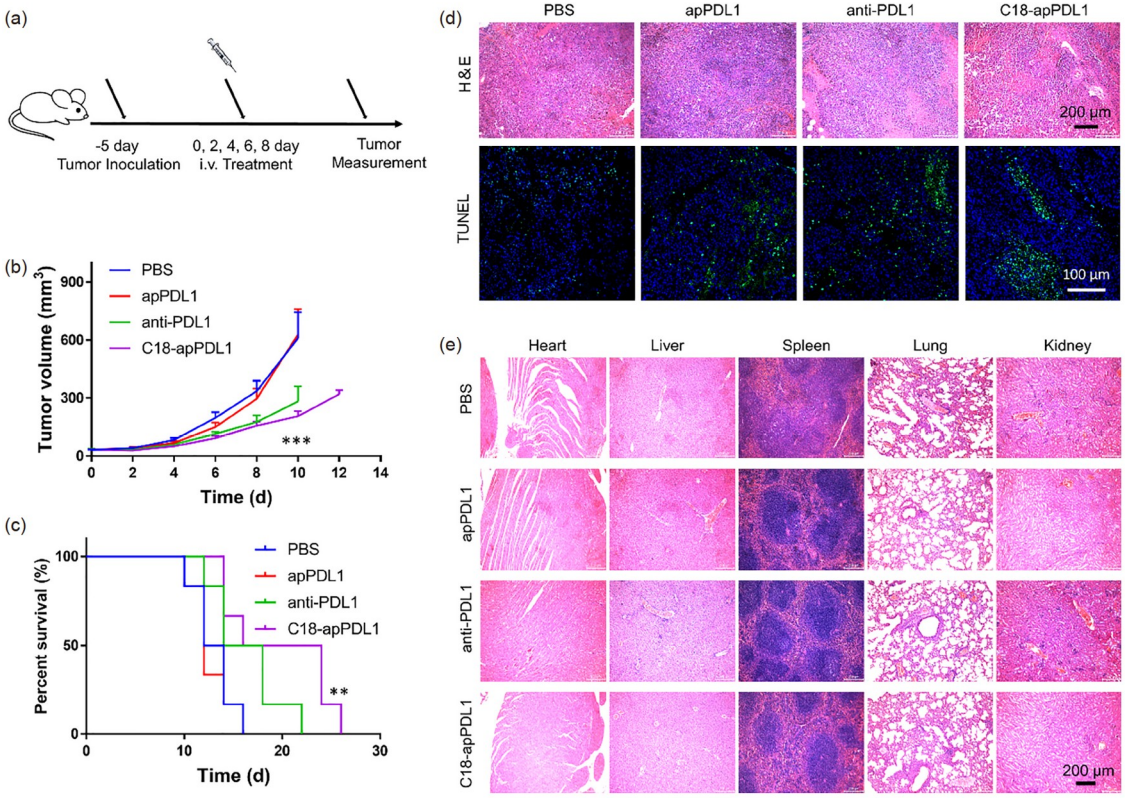

Figure 5 *In vivo* cancer immunotherapy with C18-apPDL1 in B16 tumor-bearing C57BL/6 mice. (a) Experimental design of cancer immunotherapy with C18-apPDL1. (b) Tumor growth curves after PBS, apPDL1, anti-PDL1, and C18-apPDL1 treatments at every other day five times. (c) Mice survival curves after the various treatments. (d) H&E- and TUNEL-stained tumor slices of the mice three days after the fifth treatment. (e) H&E-stained slices of the major organs three days after the fifth treatment. Error bars denote SEM. *P* values were calculated by ANOVA (**$p < 0.01$ and ***$p < 0.001$) (color online).

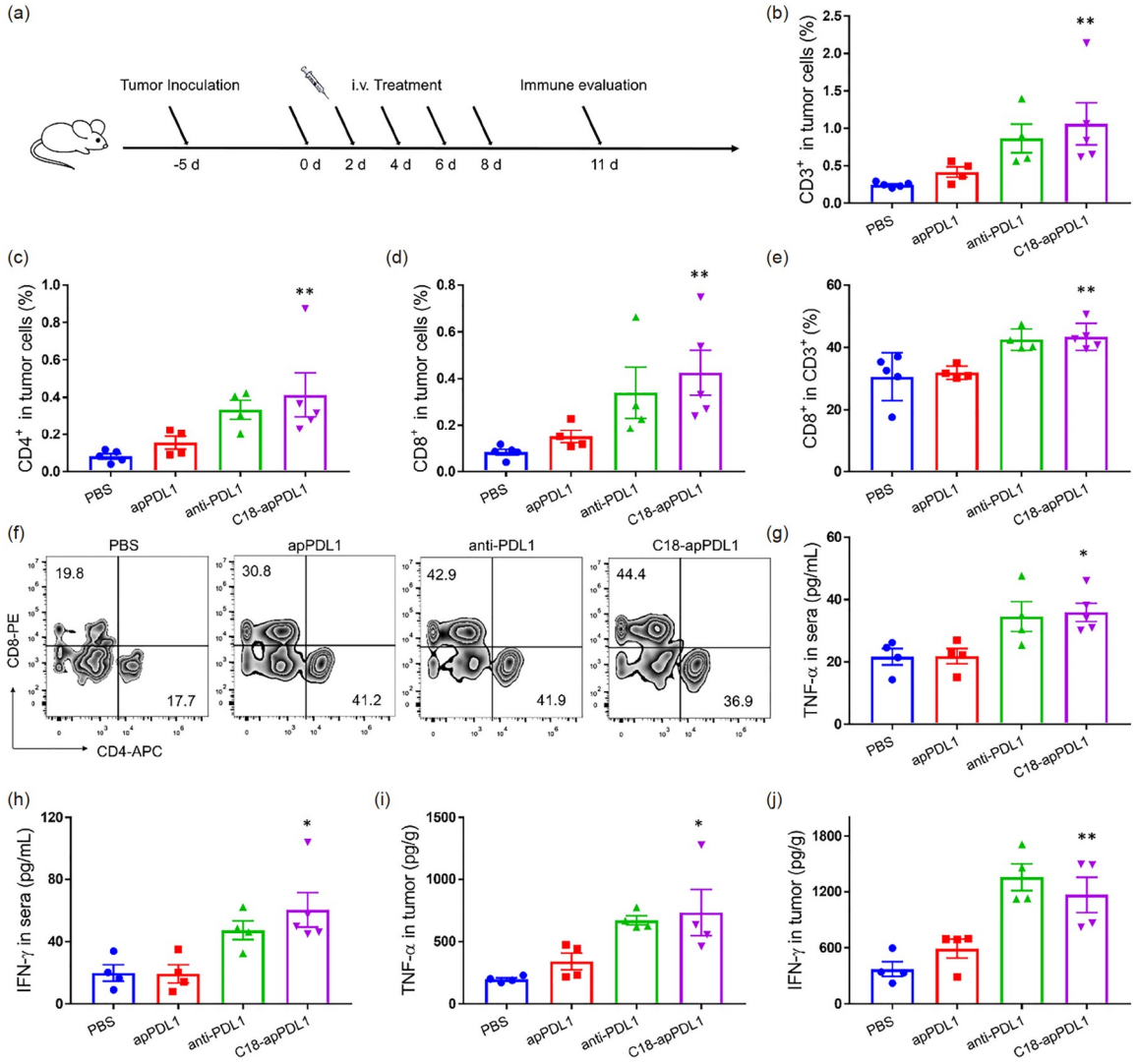

Figure 6 Immune activation after C18-apPDL1 treatments in B16 tumor-bearing C57BL/6 mice. (a) Experimental design to evaluate the tumor immune microenvironment after the treatment with C18-apPDL1. (b) $CD3^+$, (c) $CD4^+$, and (d) $CD8^+$ immune cell percentages in the tumors after the PBS, apPDL1, anti-PDL1, and C18-apPDL1 treatments. (e) Representative percentages and (f) flow cytometry plots of the $CD8^+$ T cells among the $CD3^+$ cells in the tumors after the various treatments. (g–j) Cytokines TNF-α and IFN-γ levels in the mice sera and tumors after the various treatments. Error bars denote SEM. *P* values were calculated by ANOVA (*$p < 0.05$, **$p < 0.01$, and ***$p < 0.001$) (color online).

valuable types of cytokines that are secreted by activated T cells, were measured after the various treatments (Figure 6g–j). Compared with the control and apPDL1-treated groups, the C18-apPDL1 and anti-PDL1 antibody treatments remarkably increased the cytokine levels in the mouse sera and tumors. These results together proved that C18-apPDL1 treatments could activate the immune system of a host to facilitate strong antitumor immune responses, thereby demonstrating that C18-apPDL1 could be a substitute for anti-PDL1 antibodies in cancer immunotherapy.

4 Conclusions

In summary, lipid-aptamer conjugates were prepared *via* the solid-phase DNA synthesis method. The lipid modified PDL1 aptamer could rapidly bind with albumin without weakening its binding affinity with the PDL1 protein, and it exhibited prolonged blood circulation time and enhanced *in vivo* stability postintravenous injection. Further, the ^{99m}Tc-labeled lipid-modified PDL1 aptamer as a nuclear imaging agent exhibited high tumor-homing ability because of its binding with PDL1, and it could be applied to the monitoring of the changes in PDL1 expression in tumors post-chemotherapy and radiotherapy. This lipid modified PDL1 aptamer greatly delayed tumor growth and rivaled commercial PDL1 antibodies at the same weight doses in cancer immunotherapy. Thus, this article presented the lipid-aptamer conjugate as a candidate for cancer immunoimaging and immunotherapy.

Acknowledgements This work was supported by the National Natural Science Foundation of China (32101149, 91959104, 21927803, 52032008, 51903182, 51572180), the China Postdoctoral Science Foundation (2020M671143), a Project Funded by the Priority Academic Program Development (PAPD) of Jiangsu Higher Education Institutions, Jiangsu Social Development Project (BE2019658) and Suzhou Key Laboratory of Nanotechnology and Biomedicine, Collaborative Innovation Center of Suzhou Nano Science & Technology, the Program of Introducing Talents of Discipline to Universities of China. We also thank the website of app.Biorender.com for drawing figures.

Conflict of interest The authors declare no conflict of interest.

Supporting information The supporting information is available online at http://chem.scichina.com and http://link.springer.com/journal/11426. The supporting materials are published as submitted, without typesetting or editing. The responsibility for scientific accuracy and content remains entirely with the authors.

1 Kong RM, Zhang XB, Chen Z, Tan W. *Small*, 2011, 7: 2428–2436
2 Zhang D, Zheng Y, Lin Z, Liu X, Li J, Yang H, Tan W. *Angew Chem Int Ed*, 2020, 59: 12022–12028
3 Yi X, Zhou H, Chao Y, Xiong S, Zhong J, Chai Z, Yang K, Liu Z. *Sci Adv*, 2020, 6: eaba3546
4 Fang X, Wu X, Li Z, Jiang L, Lo WS, Chen G, Gu Y, Wong WT. *Adv Sci*, 2021, 8: 2003041
5 Kuai R, Singh PB, Sun X, Xu C, Hassani Najafabadi A, Scheetz L, Yuan W, Xu Y, Hong H, Keskin DB, Wu CJ, Jain R, Schwendeman A, Moon JJ. *Adv Therap*, 2020, 3: 2000094
6 Lv G, Sun X, Qiu L, Sun Y, Li K, Liu Q, Zhao Q, Qin S, Lin J. *J Nucl Med*, 2020, 61: 117–122
7 Xu M, Han Y, Liu G, Xu Y, Duan D, Liu H, Du F, Luo P, Liu Z. *Mol Pharm*, 2018, 15: 4426–4433
8 Xing S, Lu Z, Huang Q, Li H, Wang Y, Lai Y, He Y, Deng M, Liu W. *Theranostics*, 2020, 10: 10262–10273
9 Tian L, Wang Y, Sun L, Xu J, Chao Y, Yang K, Wang S, Liu Z. *Matter*, 2019, 1: 1061–1076
10 Ren J, Xu M, Chen J, Ding J, Wang P, Huo L, Li F, Liu Z. *Theranostics*, 2021, 11: 304–315
11 Xu C, Jiang Y, Huang J, Huang J, Pu K. *Adv Mater*, 2021, 33: 2101410
12 Zhang C, Zeng Z, Cui D, He S, Jiang Y, Li J, Huang J, Pu K. *Nat Commun*, 2021, 12: 2934
13 Jiang Y, Huang J, Xu C, Pu K. *Nat Commun*, 2021, 12: 742
14 Wang Y, Song G, Liao S, Qin Q, Zhao Y, Shi L, Guan K, Gong X, Wang P, Yin X, Chen Q, Zhang XB. *Angew Chem Int Ed*, 2021, 60: 19779–19789
15 Mayer AT, Gambhir SS. *J Nucl Med*, 2018, 59: 1174–1182
16 Xu L, Wang Y, Ma Y, Huan S, Song G. *ChemMedChem*, 2021, 16: 2547–2557
17 Wang P, Kim T, Harada M, Contag C, Huang X, Smith BR. *Nanoscale Horiz*, 2020, 5: 628–653
18 Luo H, Hernandez R, Hong H, Graves SA, Yang Y, England CG, Theuer CP, Nickles RJ, Cai W. *Proc Natl Acad Sci USA*, 2015, 112: 12806–12811
19 Truillet C, Oh HLJ, Yeo SP, Lee CY, Huynh LT, Wei J, Parker MFL, Blakely C, Sevillano N, Wang YH, Shen YS, Olivas V, Jami KM, Moroz A, Jego B, Jaumain E, Fong L, Craik CS, Chang AJ, Bivona TG, Wang CI, Evans MJ. *Bioconj Chem*, 2018, 29: 96–103
20 Zhong Y, Ma Z, Wang F, Wang X, Yang Y, Liu Y, Zhao X, Li J, Du H, Zhang M, Cui Q, Zhu S, Sun Q, Wan H, Tian Y, Liu Q, Wang W, Garcia KC, Dai H. *Nat Biotechnol*, 2019, 37: 1322–1331
21 Cheng S, Jacobson O, Zhu G, Chen Z, Liang SH, Tian R, Yang Z, Niu G, Zhu X, Chen X. *Eur J Nucl Med Mol Imag*, 2019, 46: 948–956
22 Zhang X, Wu Y, Zeng Q, Xie T, Yao S, Zhang J, Cui M. *J Med Chem*, 2021, 64: 4179–4195
23 Kang L, Li C, Rosenkrans ZT, Huo N, Chen Z, Ehlerding EB, Huo Y, Ferreira CA, Barnhart TE, Engle JW, Wang R, Jiang D, Xu X, Cai W. *Adv Sci*, 2021, 8: 2001879
24 Li M, Wei W, Barnhart TE, Jiang D, Cao T, Fan K, Engle JW, Liu J, Chen W, Cai W. *Eur J Nucl Med Mol Imaging*, 2021, 1–12
25 Hong H, Nayak TR, Shi S, Graves SA, Fliss BC, Barnhart TE, Cai W. *Mol Pharm*, 2014, 11: 3624–3630
26 Bensch F, van der Veen EL, Lub-de Hooge MN, Jorritsma-Smit A, Boellaard R, Kok IC, Oosting SF, Schröder CP, Hiltermann TJN, van der Wekken AJ, Groen HJM, Kwee TC, Elias SG, Gietema JA, Bohorquez SS, de Crespigny A, Williams SP, Mancao C, Brouwers AH, Fine BM, de Vries EGE. *Nat Med*, 2018, 24: 1852–1858
27 Gao H, Wu Y, Shi J, Zhang X, Liu T, Hu B, Jia B, Wan Y, Liu Z, Wang F. *J Immunother Cancer*, 2020, 8: e001156
28 Wong NC, Cai Y, Meszaros LK, Biersack HJ, Cook GJ, Ting HH, Mottaghy FM. *Am J Nucl Med Mol Im*, 2021, 11: 154–166
29 England CG, Ehlerding EB, Hernandez R, Rekoske BT, Graves SA, Sun H, Liu G, McNeel DG, Barnhart TE, Cai W. *J Nucl Med*, 2017, 58: 162–168
30 Lao YH, Phua KKL, Leong KW. *ACS Nano*, 2015, 9: 2235–2254
31 Yang S, Wen J, Li H, Xu L, Liu Y, Zhao N, Zeng Z, Qi J, Jiang W, Han W, Zu Y. *Small*, 2019, 15: 1900903
32 Guo Z, Guilfoyle RA, Thiel AJ, Wang R, Smith LM. *Nucl Acids Res*, 1994, 22: 5456–5465
33 Jani MS, Veetil AT, Krishnan Y. *Nat Rev Mater*, 2019, 4: 451–458
34 Yang Y, Xu J, Sun Y, Mo L, Liu B, Pan X, Liu Z, Tan W. *J Am Chem Soc*, 2021, 143: 8391–8401
35 Sun L, Shen F, Tian L, Tao H, Xiong Z, Xu J, Liu Z. *Adv Mater*, 2021, 33: 2007910
36 Pastor F, Berraondo P, Etxeberria I, Frederick J, Sahin U, Gilboa E, Melero I. *Nat Rev Drug Discov*, 2018, 17: 751–767
37 Zhou F, Fu T, Huang Q, Kuai H, Mo L, Liu H, Wang Q, Peng Y, Han D, Zhao Z, Fang X, Tan W. *J Am Chem Soc*, 2019, 141: 18421–18427
38 Yang W, Liu X, Li H, Zhou J, Chen S, Wang P, Li J, Yang H. *CCS Chem*, 2021, 3: 1178–1186
39 Pilati D, Howard KA. *Expert Opin Drug Metab Toxicol*, 2020, 16: 783–795
40 Sasaki K, Ishihara J, Ishihara A, Miura R, Mansurov A, Fukunaga K, Hubbell JA. *Sci Adv*, 2019, 5: eaaw6081
41 Zhu G, Lynn GM, Jacobson O, Chen K, Liu Y, Zhang H, Ma Y, Zhang F, Tian R, Ni Q, Cheng S, Wang Z, Lu N, Yung BC, Wang Z, Lang L, Fu X, Jin A, Weiss ID, Vishwasrao H, Niu G, Shroff H, Klinman DM, Seder RA, Chen X. *Nat Commun*, 2017, 8: 1954
42 Irby D, Du C, Li F. *Mol Pharm*, 2017, 14: 1325–1338
43 Bhuniya S, Moon H, Lee H, Hong KS, Lee S, Yu DY, Kim JS. *Biomaterials*, 2011, 32: 6533–6540
44 Lacroix A, Edwardson TGW, Hancock MA, Dore MD, Sleiman HF. *J Am Chem Soc*, 2017, 139: 7355–7362
45 Wu Y, Sefah K, Liu H, Wang R, Tan W. *Proc Natl Acad Sci U S A*, 2010, 107: 5–10
46 Jin C, Zhang H, Zou J, Liu Y, Zhang L, Li F, Wang R, Xuan W, Ye M, Tan W. *Angew Chem Int Ed*, 2018, 57: 8994–8997
47 Palte MJ, Raines RT. *J Am Chem Soc*, 2012, 134: 6218–6223
48 Li X, Feng K, Li L, Yang L, Pan X, Yazd HS, Cui C, Li J, Moroz L, Sun Y, Wang B, Li X, Huang T, Tan W. *Natl Sci Rev*, 2020, 7: 1933–1953
49 Lai WY, Huang BT, Wang JW, Lin PY, Yang PC. *Mol Ther-Nucl Acids*, 2016, 5: e397
50 Prodeus A, Abdul-Wahid A, Fischer NW, Huang EHB, Cydzik M, Gariépy J. *Mol Ther-Nucl Acids*, 2015, 4: e237